



HAL
open science

Increasing sensitivity of terrestrial nitrous oxide emissions to precipitation variations

Yuanyuan Huang, Philippe Ciais, Olivier Boucher, Ying-Ping Wang, Hanqin Tian, Feng Zhou, Jinfeng Chang, Zhaolei Li, Daniel S. Goll, Ray Langenfelds, et al.

► **To cite this version:**

Yuanyuan Huang, Philippe Ciais, Olivier Boucher, Ying-Ping Wang, Hanqin Tian, et al.. Increasing sensitivity of terrestrial nitrous oxide emissions to precipitation variations. *Environmental Research: Climate*, 2022, 1, 10.1088/2752-5295/aca2d1 . insu-03993083

HAL Id: insu-03993083

<https://insu.hal.science/insu-03993083>

Submitted on 16 Feb 2023

HAL is a multi-disciplinary open access archive for the deposit and dissemination of scientific research documents, whether they are published or not. The documents may come from teaching and research institutions in France or abroad, or from public or private research centers.

L'archive ouverte pluridisciplinaire **HAL**, est destinée au dépôt et à la diffusion de documents scientifiques de niveau recherche, publiés ou non, émanant des établissements d'enseignement et de recherche français ou étrangers, des laboratoires publics ou privés.

PAPER • OPEN ACCESS

Increasing sensitivity of terrestrial nitrous oxide emissions to precipitation variations

To cite this article: Yuanyuan Huang *et al* 2022 *Environ. Res.: Climate* 1 025010

View the [article online](#) for updates and enhancements.

You may also like

- [Long-term ENSO prediction with echo-state networks](#)
Forough Hassanibesheli, Jürgen Kurths and Niklas Boers
- [Weather drives variation in COVID-19 transmission and detection](#)
James Rising, Manuel Linsenmeier and Ana De Menezes
- [Heat exposure and resilience planning in Atlanta, Georgia](#)
Nkosi Muse, David M Iwaniec, Chris Wyczalkowski et al.

ENVIRONMENTAL RESEARCH CLIMATE



PAPER

Increasing sensitivity of terrestrial nitrous oxide emissions to precipitation variations

OPEN ACCESS

RECEIVED
5 July 2022

REVISED
3 November 2022

ACCEPTED FOR PUBLICATION
15 November 2022

PUBLISHED
1 December 2022

Original content from this work may be used under the terms of the [Creative Commons Attribution 4.0 licence](#).

Any further distribution of this work must maintain attribution to the author(s) and the title of the work, journal citation and DOI.



Yuanyuan Huang^{1,2,*} , Philippe Ciais³ , Olivier Boucher⁴, Ying-Ping Wang² , Hanqin Tian⁵ , Feng Zhou⁶ , Jinfeng Chang⁷ , Zhaolei Li⁸, Daniel S Goll⁹, Ray Langenfelds², Hao Shi¹⁰ , Naiqing Pan¹⁰, Hang-Wei Hu¹¹, Shu Kee Lam¹¹ and Ning Dong¹²

¹ Laboratoire de Météorologie Dynamique, IPSL, École polytechnique, Palaiseau, France

² Now at CSIRO Oceans and Atmosphere, Aspendale 3195, Australia

³ Laboratoire des Sciences du Climat et de l'Environnement, LSCE/IPSL, CEA-CNRS-UVSQ, Université Paris-Saclay, 91191 Gif-sur-Yvette, France

⁴ Institut Pierre-Simon Laplace, Sorbonne université / CNRS, 4 place Jussieu, 75005 Paris, France

⁵ Schiller Institute for Integrated Science and Society, Department of Earth and Environmental Sciences, Boston College, Chestnut Hill, MA 02467, USA

⁶ Sino-France Institute of Earth Systems Science, Laboratory for Earth Surface Processes, College of Urban and Environmental Sciences, Peking University, Beijing, China

⁷ College of Environmental and Resource Sciences, Zhejiang University, Hangzhou, China

⁸ College of Resources and Environment, and Academy of Agricultural Sciences, Southwest University, Chongqing 400715, China

⁹ Université Paris Saclay, CEA-CNRS-UVSQ, LSCE/IPSL, Gif sur Yvette, France

¹⁰ International Center for Climate and Global Change Research, School of Forestry and Wildlife Sciences, Auburn University, Auburn, AL, USA

¹¹ School of Agriculture and Food, The University of Melbourne, Victoria 3010, Australia

¹² Georgina Mace Centre for the Living Planet, Imperial College London, Department of Life Sciences, Silwood Park Campus, Ascot SL5 7PY, UK

* Author to whom any correspondence should be addressed.

E-mail: yuanyuanhuang2011@gmail.com

Keywords: sensitivity, terrestrial, nitrous oxide, precipitation

Supplementary material for this article is available [online](#)

Abstract

Nitrous oxide (N₂O), a major greenhouse gas and ozone-depleting agent, is generated over land mostly from two key biochemical processes—nitrification and denitrification. Nitrifying and denitrifying N₂O production occurs preferably under alternative oxic and anoxic conditions, which are closely linked with variations in water filled soil pores, and thus indirectly with precipitation. We show here that the interannual anomalies in the annual growth rate of the global land N₂O emissions are significantly ($P < 0.001$) correlated with precipitation anomalies, with an overall sensitivity (α^{PRE} , changes of land N₂O emission variations per precipitation anomalies) of 2.50 ± 0.98 Tg N₂O–N per 100 mm of precipitation across the global land (1998–2016). The sensitivity (α^{PRE}) and precipitation-driven N₂O anomalies increased during 1998–2016, partly due to increased nitrogen inputs to agricultural lands and enhanced precipitation anomalies. Spatially, we find that the α^{PRE} increases with aridity. We predict a larger α^{PRE} under future climate conditions (with radiative forcing levels of 4.5, 7.0 and 8.5 Wm⁻²) by the year 2100 if nitrogen fertilization follows the present practice.

1. Introduction

Nitrous oxide (N₂O) is a major long-lived greenhouse gas and ozone-depleting substance, whose atmospheric concentration has been increasing since the mid-eighteenth century. Human induced surplus (i.e. beyond biological demands) of reactive nitrogen, through, for example, the Haber-Bosch process (the main industrial procedure to produce synthetic nitrogen fertilizers) and expansion of nitrogen-fixing crops, is one of the major drivers of the increasing trend. This trend is expected to continue into the future due to the growing demand for food, feed, fuel and fibre [1]. While there is a strong scientific consensus on the

increasing trend of land N₂O emissions and its origin, the year-to-year variations in the growth rate of emissions and their drivers at the global scale remain largely unknown.

Nitrification and denitrification are the two major biochemical processes (mostly controlled by microorganisms) that produce N₂O in terrestrial and aquatic ecosystems. Nitrification is an aerobic process from which ammonium is oxidized to form nitrate. N₂O is produced as a by-product during this process. Denitrification, which includes heterotrophic denitrification, nitrifier denitrification, chemodenitrification (abiotic) and codenitrification (biotic) [2], reduces oxidized forms of nitrogen (e.g. nitrate) to produce a series of gaseous nitrogen species, including N₂O, and requires low oxygen conditions. Nitrification and denitrification, as well as their associated gaseous N₂O emissions, are sensitive to multiple environmental drivers. Temperature, soil water, redox potential (or oxygen levels), nitrogen availability (therefore nitrogen fertilizer input), carbon supply and soil pH are common regulators of land N₂O emissions documented across laboratory, field and modelling studies [2–5]. How those abiotic and biotic, human induced and natural factors control land N₂O emissions are complex. N₂O fluxes are highly heterogeneous in space and time [3, 6]. The water filled pore space, sometimes represented by soil moisture, plays a particularly important role as it controls nitrification and denitrification rates through regulating the substrate availability and soil redox potential (oxygen diffusion rates are much slower in water-filled than air-filled pore space), and also alters the partitioning among gaseous nitrification and denitrification products (e.g. NO, N₂O and N₂) [5, 7]. Most well-known hot (with disproportionately high intensity) spots and moments of emissions, such as those at the terrestrial-aquatic interface, riparian zones, oxic–anoxic interfaces of drained organic soils, or/and triggered by rainfall and freeze-thaw events, are related to water availability [8].

Recent climate change has altered precipitation regimes across large areas of the global land, resulting in an increasing frequency of both dry and wet spells, as reflected in soil moisture anomalies [9, 10]. Field observations show relatively low N₂O flux under dry conditions and high emissions following rewetting, partly due to the accumulation of organic nitrogen or/and nitrate during the preceding dry periods that favour denitrifying N₂O productions under wet conditions [11, 12]. Using an inverse procedure combining flux tower measurements, Griffis *et al* [4] showed enhanced N₂O emissions during warm and wet periods in the US Corn Belt. The notorious heterogeneity of land N₂O emissions in space and time makes it difficult to upscale sparse local observations to derive global patterns and drivers. Regional and global studies on the response of land N₂O emissions to precipitation are scarce. From the N₂O Model Intercomparison Project (NMIP) [13], under idealized simulations where only climate was varied temporally, the anomaly (difference compared to the emission in 1901) of global land N₂O emissions were simulated to increase with time (Extended Data figure 8 of [14]) in association with warming since the industrial revolution. It remains unclear from this correlation with temperature trends whether the imprint of precipitation on global land N₂O emissions is muted due to averaging of different trends across space, or whether the signal has yet to be detected.

We hypothesize that the interannual anomalies in the growth rate of the global land N₂O emissions are correlated with precipitation anomalies. At least two lines of arguments support our hypothesis. Theoretically, nitrifying–denitrifying N₂O production is favoured under alternative aerobic and anaerobic conditions, which could be mediated by precipitation [3, 15–17]. Empirically, laboratory and field observations have revealed the strong linkages between water availability and N₂O production processes [16–18]. Here and afterwards, we use N₂OEA (nitrous oxide emission anomalies) to refer to the interannual anomalies in the growth rate of land N₂O emissions, calculated through a 12 month moving sum window over the detrended (linear least-squares fitting) monthly growth rate of emissions [19]. The growth rate of a specific month is the difference between the N₂O flux in that month and in the same month of the previous year (see Methods) [20]. Climate anomalies (PRE: precipitation; TEMP: temperature; RAD: solar radiation) were calculated using the same procedure.

2. Methods

2.1. Land N₂O emissions

Land N₂O emissions were derived from three independent atmospheric inversion systems, i.e. TOMCAT (1998–2014), LMDz (1998–2016) and MIROC4-ACTM (1998–2016) [19]. These systems apply the Bayesian inversion to optimally combine observed N₂O mixing ratios from discrete air samples and *in-situ* instrument networks with atmospheric transports, which account for processes such as the loss of N₂O in the stratosphere caused by photolysis and oxidation by O (¹D). The inversions generate grid-level land N₂O emissions at a monthly temporal resolution. The land here also includes the inland water bodies due to the difficulty of separating them with relatively coarse grid cell resolution (>100 km × 100 km). Detailed information for the inversion products is available in [19]. To quantify the global or regional budgets, we integrated the gridded emissions through corresponding land areas. To estimate land N₂O emissions, we

removed anthropogenic emissions from the energy, industry and waste sectors using the PRIMAP-hist historical emission database [21], despite this not having a noticeable effect on the general relationship between anomalies of N₂O emissions and precipitation (supplementary figure 1). Keeping vs. removing biomass burning emissions using GFED-v4.1 s did not change the global pattern between land N₂O emissions and precipitation anomalies noticeably (supplementary figure 1). For the global budget, we reported results that exclude biomass burning emissions.

We also analyzed land N₂O emissions from process-based land models that participated in the NMIP project [13]. Three models (namely, ORCHIDEE-CNP, ORCHIDEE and OCN) provided simulations with the same temporal resolutions as the atmospheric inversions. Model simulations share the same experimental protocol, e.g. with the same climate drivers Climatic Research Unit-National Centers for Environmental Prediction (CRU-NCEP), land use (HYDE version 3.2) and anthropogenic nitrogen inputs. Nitrogen fertilizer input integrates country-level fertilizer statistics (yearly) from the International Fertilizer Industry Association and the Food and Agriculture Organization, with detailed information from [22]. The timing and splitting frequency of fertilizer application depend on model assumptions, such as one application at the beginning of the growing season.

2.2. Climate data

Gridded climate data used in this study includes aridity, monthly mean land surface air temperature, precipitation and solar radiation. We used the gridded (0.5° × 0.5°) CRU time-series (TS) data version 4.04 (CRU TS4.04)[23], provided by CRU at the University of East Anglia as our climate dataset for temperature, precipitation and solar radiation. CRU TS4.04 does not include solar radiation, and we therefore used the cloud cover to approximate variations in solar radiation. We also applied the CRU-NCEP dataset (<https://rda.ucar.edu/datasets/ds314.3/>) as an alternative for temperature, precipitation and especially for solar radiation. CRU-NCEP combines observations from CRU with the NCEP-NCAR reanalysis data products, and was applied as meteorological forcing data in NMIP. Solar radiation in CRU-NCEP was corrected to match empirically derived monthly solar radiations based on latitude and sunshine hours, which is correlated with the CRU cloud fraction. To test the robustness of the relationship between precipitation and land N₂O emissions and to quantify the uncertainty, we included 3 other precipitation datasets that combine different sources of rain gauge stations, satellites, sounding observations and reanalyses. The Global Precipitation Climatology Centre (GPCC) provides quality-controlled monthly data from 7,000–9,000 stations (www.dwd.de/EN/ourservices/gpcc/gpcc.html). GPCC v2018 was obtained from (<https://psl.noaa.gov/data/gridded/data.gpcc.html>) (assessed Jan 2021). GPCPv2.3 (<https://climatedataguide.ucar.edu/climate-data/gpcp-monthly-global-precipitation-climatology-project>, assessed Jan 2021) is the Global Precipitation Climatology Project monthly precipitation dataset from 1979-present that combines observations and satellite precipitation data into 2.5° × 2.5° global grids. NOAA's Precipitation Reconstruction over Land (NOAA, <https://psl.noaa.gov/data/gridded/data.precl.html>, assessed Jan 2021) provides 1° × 1° global grids of monthly precipitation reconstructed from observations over 17 000 gauge stations.

We separated the global land into hyperarid, arid, semi-arid, dry subhumid and humid regions based on the aridity index. Aridity index here is defined as the ratio between precipitation and the reference evapotranspiration, provided by [24]. Hyperarid region is classified as the land with the smallest aridity index (AI < 0.03) and covers 7.5% of the total global land area according to the United Nations Environment Programme [25]. The class with the second smallest aridity index (AI: 0.03–0.2) is the arid region, which covers 12.1% of the global land, followed by semi-arid (17.7% of land area, AI: 0.2–0.5), dry subhumid (9.9%, AI: 0.5–0.65) and humid regions (52.8%, AI > 0.65). All gridded datasets (climate and N₂O) were regridded to 1° × 1° using the nearest neighbourhood method for consistency.

Projections of 5 Earth system models (CESM2-WACCM, ACCESS-CM2, GFDL-ESM4, IPSL-CM6A-LR, MIROC6) under SSP5-85, SSP3-70, SSP2-45 and SSP1-26 from the ScenarioMIP [26] serve to quantify future changes in precipitation anomalies.

2.3. Anomalies, sensitivities and decompositions

The growth rate of land N₂O emissions of a specific month was calculated as the difference between N₂O emissions from that specific month and the month in the previous year. The monthly growth rates were detrended (linear least-squares fitting) and summed every 12 months to estimate the interannual anomalies (N₂OEA) similarly as in [20]. Interannual anomalies of climate variables (PRE: precipitation; TEMP: temperature; RAD: solar radiation) were calculated in a similar way. Current available global datasets of anthropogenic nitrogen inputs are coarse in temporal resolution (yearly), with the signal dominated by the increasing trend in the past several decades. The direct impact of the anomaly of nitrogen inputs alone is less likely to be the major driver of N₂OEA as the anomaly signal of nitrogen inputs is small after detrending. Instead, N₂OEA are more likely to be driven by anomalies in climate or/and its interactions with

anthropogenic nitrogen inputs. We calculated the time-lag (within 12 months) in which the highest Pearson correlation coefficient between N₂OEA and PRE was obtained. We reported results with optimum time-lags. Calculations with vs. without time-lags yield similar results (α^{PRE} and N₂OEA_PRE) and patterns discovered in this study are robust.

The sensitivity (α^{PRE}) of N₂OEA to PRE was quantified as the slope of PRE in the multiple regression of N₂OEA against anomalies of precipitation, temperature and radiation. The significance of the regression slope was analyzed through the *t*-test. For the global total N₂OEA, we tested incorporating total nitrogen fertilizer (both detrended and not detrended) as an independent predictor, or/and as a predictor interacting with different combinations of climate variables. In the tests, we assumed an equal application rate of nitrogen fertilizer each month with only annual nitrogen fertilization statistics and no comprehensive information on the timing of applications at the global scale. We did not find a noticeable improvement in the performance of the regression (*R*² did not increase) and precipitation remained as the dominant predictor. We therefore focused on the first order effects and reported results on the partial linear regression with only precipitation, temperature and radiation as predictors (supplementary figure 2). We calculated α^{PRE} over a moving time window of 96 months and tested the significance of the trends through the Mann–Kendall method. To verify that the trends are not specific to the moving window length, we varied the window length from 48 to 144 months. And we found similar trends. N₂OEA has an autocorrelation of around 6 months. To test whether our analyses were impacted by the autocorrelation, we calculated α^{PRE} through the generalized linear mixed model (GLMM: allow for flexible nonnormal distributions of data) that explicitly considers the temporal autocorrelation utilizing the first-order autocorrelation function (i.e. accounts for correlations among the consecutive data points.)

Considering autocorrelation had a minor impact on α^{PRE} (supplementary figure 3). In addition, to test whether our results are specific to the detrending method, we applied the singular spectrum analysis, a nonparametric spectral estimation method for TS analysis, and found a similar increase in α^{PRE} (supplementary figure 4).

For the contributions of precipitation to N₂OEA, in addition to α^{PRE} , variations in precipitation also play a role. We decomposed variations of climate-driven N₂OEA into contributions from precipitation (N₂OEA_PRE), temperature (N₂OEA_TEMP) and radiation (N₂OEA_RAD) similarly as in [27]:

$$\text{N}_2\text{OEA}_{d,t} = \alpha_d^{\text{PRE}} \times \text{PRE}_{d,t} + \alpha_d^{\text{TEMP}} \times \text{TEMP}_{d,t} + \alpha_d^{\text{RAD}} \times \text{RAD}_{d,t} + \varepsilon_{d,t} \quad (1)$$

$$\text{N}_2\text{OEA}_{d,t} \approx \text{N}_2\text{OEA_PRE}_{d,t} + \text{N}_2\text{OEA_TEMP}_{d,t} + \text{N}_2\text{OEA_RAD}_{d,t} \quad (2)$$

where α_d with the superscript is the sensitivity of N₂OEA to the corresponding climate anomalies (PRE, TEMP and RAD). *d* indicates one set of climate and N₂O data. *t* indicates time. $\varepsilon_{d,t}$ is the residue term. The product of the sensitivity and the corresponding climate anomaly gives the N₂O anomaly component driven by that climate anomaly. For example, $\text{N}_2\text{OEA_PRE}_{d,t} = \alpha_d^{\text{PRE}} \times \text{PRE}_{d,t}$, which quantifies the contribution of precipitation anomaly to N₂O flux anomaly. We estimated contributions of each climate driver both at the global scale through globally integrated fluxes and individually for each grid cell. To compare the magnitude of anomalies among locations or time-windows, we calculated the standard deviation of each anomaly TS. We used $\text{N}_2\text{OEA_PRE}_d^{\text{STD}}$, $\text{N}_2\text{OEA_TEMP}_d^{\text{STD}}$ and $\text{N}_2\text{OEA_RAD}_d^{\text{STD}}$ to denote the standard deviation of $\text{N}_2\text{OEA_PRE}_d^{\text{STD}}$, $\text{N}_2\text{OEA_TEMP}_d^{\text{STD}}$ and $\text{N}_2\text{OEA_RAD}_d^{\text{STD}}$. For simplicity, we neglect the subscript *d* and adopted the notation $\text{N}_2\text{OEA_PRE}_d^{\text{STD}}$, $\text{N}_2\text{OEA_TEMP}_d^{\text{STD}}$ and $\text{N}_2\text{OEA_RAD}_d^{\text{STD}}$ when we did not refer to a specific climate and N₂O dataset.

To estimate the uncertainties in α^{PRE} and climate-driven N₂OEA, we applied the bootstrapping method with 1000 random samples combining different data sources (five precipitation, two radiation and two temperature datasets) for each of the N₂O datasets. Uncertainties were expressed as the standard deviations of these samples.

To understand the spatial patterns and mechanisms that lead to the enhanced influence of precipitation on N₂OEA, we calculated α^{PRE} and $\text{N}_2\text{OEA_PRE}^{\text{STD}}$ across spatially aggregated groups. We first divided the global land into five categories by aridity. For each category, we further separated it into two groups by their magnitude (i.e. standard deviation) of precipitation anomalies (PRE). One group has an enhanced precipitation anomaly, shown by a higher standard deviation of PRE in the recent time window (2009–2016) than in the earliest time window (1998–2005). And the other group has reduced precipitation anomalies. We also looked into contributions from agricultural lands vs. natural lands. The atmospheric inversion estimates mix agricultural and non-agricultural emissions within a grid cell. As a coarse approximation, we used the fractional area of cropland [28] as the criterion to separate agricultural and non-agricultural lands. We define non-agricultural grid cells as locations with cropland area < 1%, whereas agricultural grid cells have

cropland areas bigger than a threshold value. Agricultural grid cells have an average mineral N input rate of $7 \text{ gN (m}^2 \text{ cropland)}^{-1} \text{ yr}^{-1}$ (1998–2013) [22].

We tested the threshold value from 20% to 50%, and found that the results of a generally higher mean $\Delta\alpha^{\text{PRE}}$ and $\Delta\text{N}_2\text{OEA_PRE}^{\text{STD}}$ in agricultural than non-agricultural lands are robust (supplementary figure 5). Δ represents the difference between the recent vs. the earliest time window. For process-based modelling estimates, agricultural N_2O fluxes due to anthropogenic nitrogen inputs were directly calculated from simulations with vs. without anthropogenic nitrogen inputs.

To derive the scale dependence of the relative importance of different climate components, we define the relative importance of a climate component as the mean variance (across space) of the anomalies of this component divided by the mean variance of the climate driven N_2OEA , following the method from [27]. For example, the relative importance of precipitation anomalies (I^{PRE}) is quantified as,

$$I^{\text{PRE}} = \frac{\mu_s (\sigma_t^2 (\text{N}_2\text{OEA_PRE}_{s,t}))}{\mu_s (\sigma_t^2 (\text{N}_2\text{OEA_PRE}_{s,t} + \text{N}_2\text{OEA_TEMP}_{s,t} + \text{N}_2\text{OEA_RAD}_{s,t}))} \quad (3)$$

where s is the index for locations (or grid cells), μ stands for the mean and σ represents the standard deviation. We then integrated N_2O and climate variables sequentially to coarser resolutions, starting from 1° , to 2° , 3° , 4° , 5° , 6° , 7° , 8° , 9° , 10° , 11° , 14° , 18° , 22° , 30° , 60° , 90° and 180° until the globe (one grid cell), and computed the climate-driven components and relative importance for each spatial resolution.

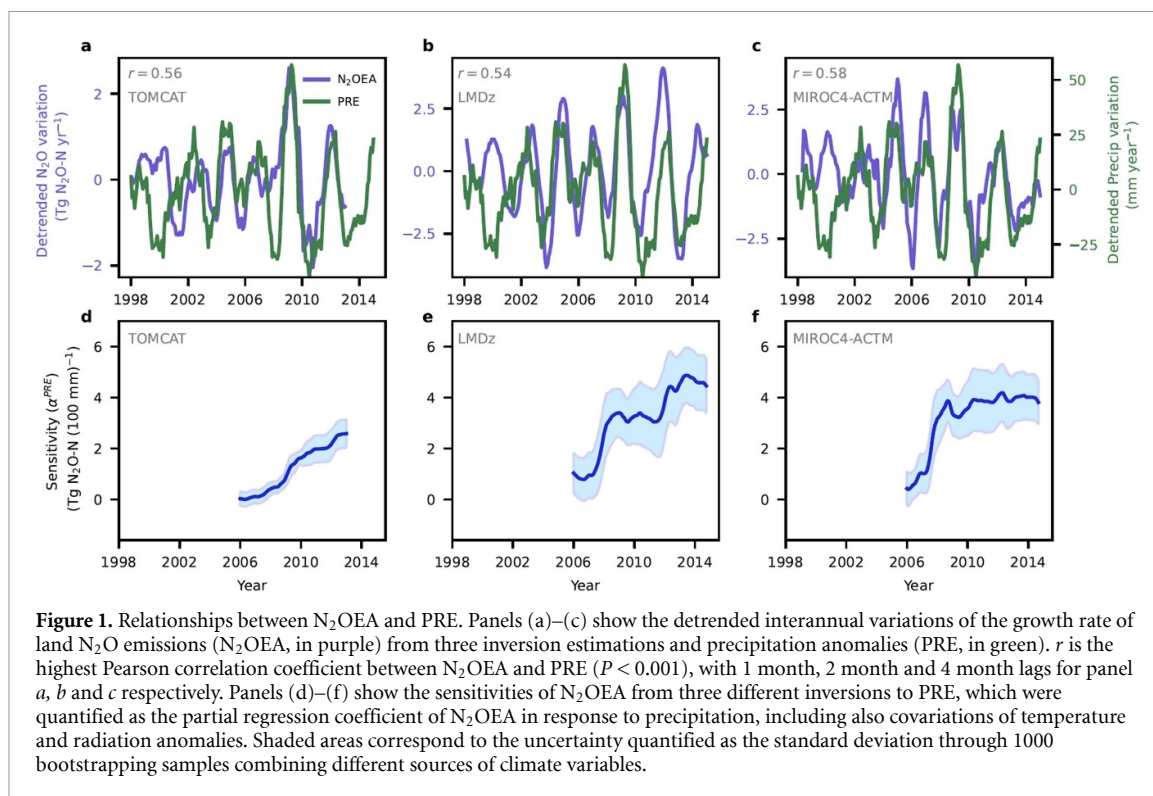
3. Results and discussions

We firstly focus on the top-down estimates of land N_2O emissions from three independent atmospheric inversion systems (TOMCAT, LMDz and MIROC4-ACTM) [19]. These inversion systems integrate measurements of atmospheric N_2O dynamics from global networks with knowledge of the sources, sinks and atmospheric transport of N_2O . Figures 1(a)–(c) shows a positive correlation between the globally integrated N_2OEA derived from atmospheric inversions and PRE (see Methods; $r = 0.56$, $P < 0.001$ for TOMCAT; $r = 0.54$, $P < 0.001$ for LMDz; $r = 0.58$, $P < 0.001$ for MIROC4-ACTM, 1998–2016), consistent with local field studies and process-based understandings of the control of water on N_2O emissions [3, 15–17].

We then quantified the sensitivity (α^{PRE}) of the globally integrated N_2OEA to PRE as the partial derivative of N_2OEA in response to PRE in the multiple regression of N_2OEA against climate variables (PRE, TEMP and RAD). We included radiation as a climate predictor considering especially its role in vegetation dynamics, which regulates the energy (carbon) and substrate (nitrogen) availability for nitrification and denitrification. With an ensemble of estimates combining the three N_2O inversions and different datasets of climate variables (Methods; PRE: 5 datasets; TEMP: 2 datasets; RAD: 2 datasets), the overall global α^{PRE} is 2.50 ± 0.98 (mean \pm standard deviation) $\text{Tg N}_2\text{O-N (100 mm)}^{-1}$ during 1998–2016. That is, a 100 mm rise in precipitation over the global land increases N_2O emissions by 2.50 ± 0.98 (t -test, $P < 0.01$) $\text{Tg N}_2\text{O-N}$.

To translate sensitivities to contributions to N_2OEA during 1998–2016, we decomposed N_2OEA into the contributions from precipitation ($\text{N}_2\text{OEA_PRE}$), temperature ($\text{N}_2\text{OEA_TEMP}$), and radiation ($\text{N}_2\text{OEA_RAD}$) (see Methods, equations (1) and (2)). Climate anomalies explain up to 59% of the globally integrated N_2OEA . More than 90% of the climate-induced variations in globally integrated N_2OEA are attributable to precipitation (supplementary figure 2). Note here we focus on the anomaly and removed the trend signal from temperature, which has been hypothesized to be an important regulator of historical land N_2O emissions. Adding nitrogen fertilization rate as a global explanatory variable (with or without interactions with climate variables) does not improve the regression performance partly due to large uncertainties in the timing and rate of fertilizer additions at the global scale (methods). To facilitate comparisons among locations, time-windows and climate variables, we use the standard deviation of $\text{N}_2\text{OEA_PRE}$ ($\text{N}_2\text{OEA_TEMP}$ and $\text{N}_2\text{OEA_RAD}$) over specific time periods to indicate the strength of the climate-driven anomalies, which we denote as $\text{N}_2\text{OEA_PRE}^{\text{STD}}$ ($\text{N}_2\text{OEA_TEMP}^{\text{STD}}$ and $\text{N}_2\text{OEA_RAD}^{\text{STD}}$) for simplicity.

Spatially, there was a large variation in α^{PRE} in different places. Roughly, we found that α^{PRE} increases with aridity (defined as the ratio between precipitation and the reference evapotranspiration [24], figure 2(b)). Hyperarid regions (e.g. Sahara and Arabian Deserts) have a high α^{PRE} averaged among pixels falling in this aridity class, but this high sensitivity does not translate into a high mean $\text{N}_2\text{OEA_PRE}^{\text{STD}}$, due to small changes in the amount and therefore in the absolute anomalies of precipitation in those regions. The standard deviation of α^{PRE} is also high in hyperarid regions likely due to limited observations and large uncertainties in estimating N_2O emissions. Humid regions, covering 52.8% of the global land area, contribute to the largest portion (54.3%) of the globally integrated $\text{N}_2\text{OEA_PRE}^{\text{STD}}$ (sum across land area), followed by the semi-arid regions (figure 2(d)). Semi-arid regions stand out for their highest

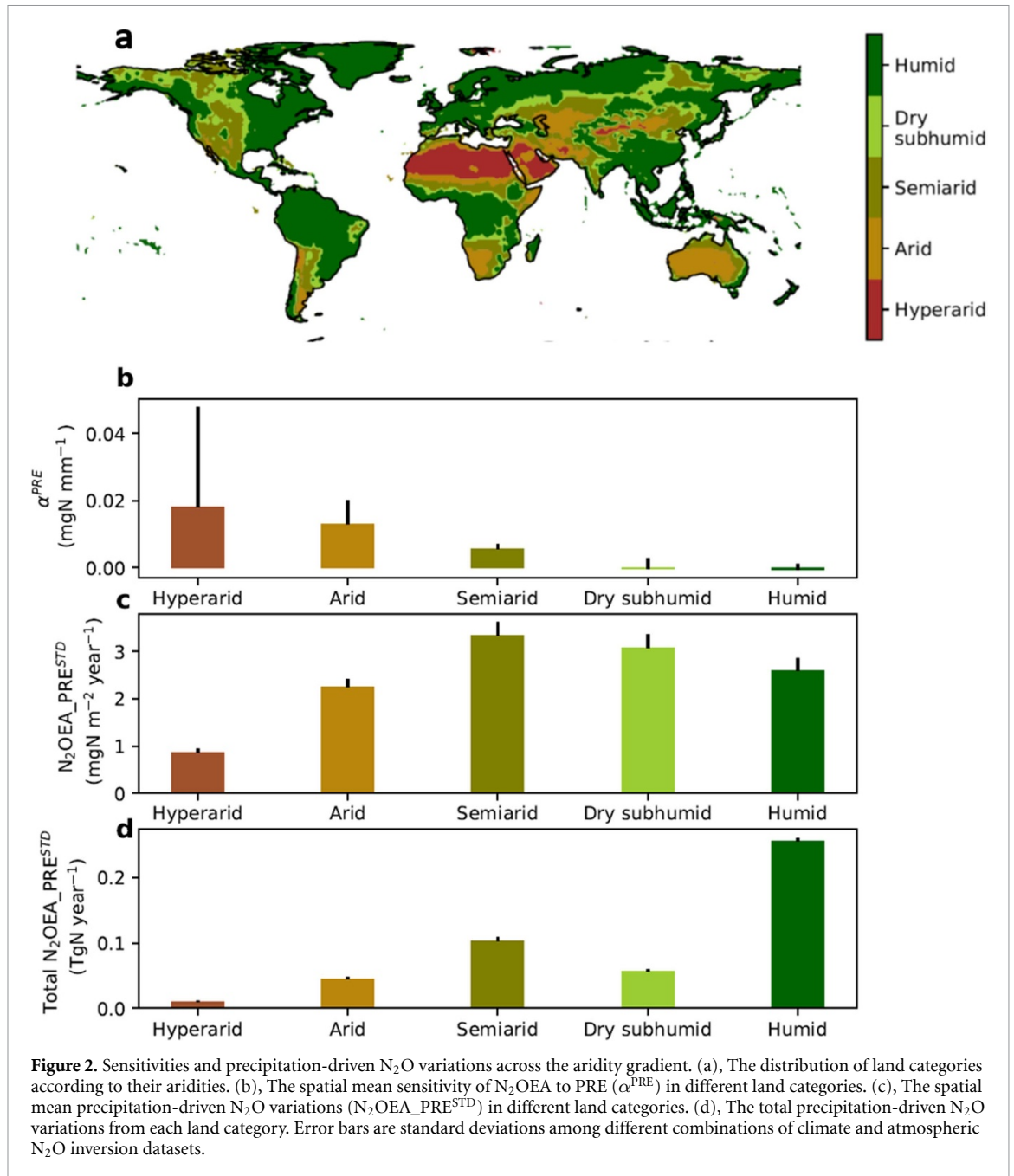


N₂OEA_PRE^{STD} per unit area ($3.33 \pm 0.28 \text{ mg N m}^{-2} \text{ yr}^{-1}$, figure 2(c)). The dominant contributions of humid (45%–48%) and semi-arid (20%–29%) regions to the global correlation between N₂OEA and PRE were also verified by calculating the contribution of each region using the additive properties of covariances (supplementary table 1).

We also found that the global α^{PRE} has increased with time during the study period from 1998 to 2016. Combining three datasets of N₂O emissions from inversions, α^{PRE} is 0.50 ± 0.73 (t -test, $P > 0.3$) in the earliest time window (first 96 months, 1998–2005), and reaches 3.63 ± 1.22 (t -test, $P < 0.001$) Tg N₂O–N (100 mm)^{−1} in the recent time period (2007–2014). Figures 1(d)–(f) displays changes of α^{PRE} over a moving time window of 96 months, with a significant (Mann–Kendall trend test, $P < 0.001$) increasing trend for all of the three atmospheric N₂O inversions. Not only the sensitivity (α^{PRE}) grows over time, but the contribution of precipitation, quantified as the standard deviation across the corresponding time window (N₂OEA_PRE^{STD}, Methods), also increases significantly over time, from 0.12 ± 0.1 – 1 ± 0.29 Tg N₂O–N yr^{−1} (supplementary figures 6(g)–(i)).

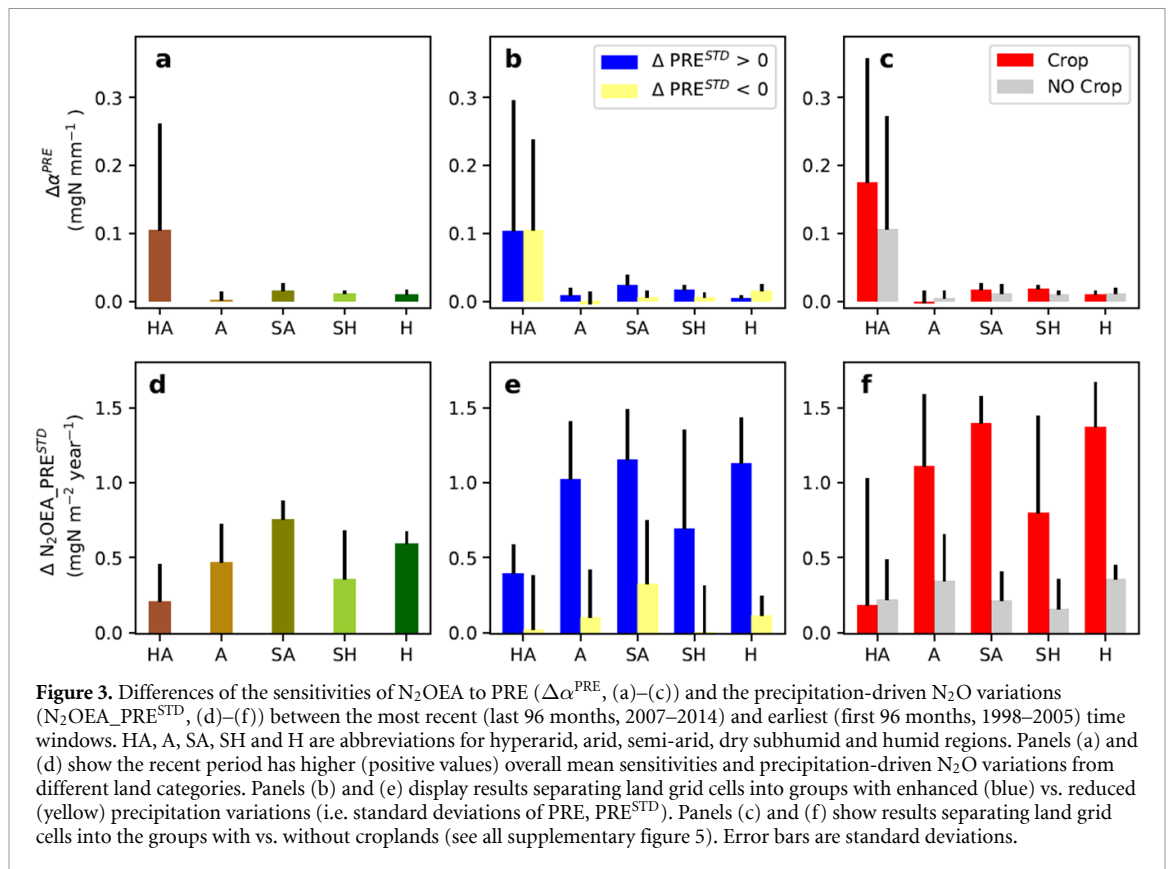
We further verified the robustness of the enhanced α^{PRE} in the study period through (a) applying the nonparametric spectral estimation method (singular spectrum analysis) to separate the trend and other components instead of the linear least-squares detrending; and (b) varying the moving window length for calculating α^{PRE} from 48 to 144 months. Note the time-span and testing window length of our study are limited by use of atmospheric N₂O measurements from the year 1998 onwards. Earlier atmospheric data have lower calibration accuracy and measurement precision [19]. We also verified that considering autocorrelation only had a minor impact on the inferred increase of α^{PRE} (Methods, supplementary figure 3). Note α^{PRE} at the beginning of the study is not statistically significant, which may be related to a larger uncertainty before 2000 [19]. After removing data from the first two years, we obtained an initial α^{PRE} of 2.05 ± 1.52 Tg N₂O–N (100 mm)^{−1} and N₂OEA_PRE^{STD} of 0.38 ± 0.25 Tg N₂O–N yr^{−1}. The increasing trend for all of the three atmospheric N₂O inversions still holds (Mann–Kendall trend test, $P < 0.001$).

To understand mechanisms underlying this enhanced α^{PRE} and the contribution of precipitation to N₂O variations, we calculated the difference of these quantities between the most recent and the earliest time windows (denoted as $\Delta\alpha^{\text{PRE}}$ and $\Delta\text{N}_2\text{OEA_PRE}^{\text{STD}}$) by region. Hyperarid, arid, semi-arid, dry subhumid and humid regions all show positive mean $\Delta\alpha^{\text{PRE}}$ and $\Delta\text{N}_2\text{OEA_PRE}^{\text{STD}}$ across grid cells (figure 3) despite large variations in $\Delta\alpha^{\text{PRE}}$ and $\Delta\text{N}_2\text{OEA_PRE}^{\text{STD}}$ locally (supplementary figure 7). We further separated the global grid cells into two groups: one group with enhanced variations in precipitation anomalies ($\Delta\text{PRE}^{\text{STD}} > 0$, STD stands for standard deviation, Δ indicates the difference between the recent vs. the initial time window) and the other with reduced anomalies in precipitation ($\Delta\text{PRE}^{\text{STD}} < 0$). In arid, semi-arid and dry subhumid regions, the grid cells that experienced intensified anomalies of precipitation show a higher mean



$\Delta\alpha^{PRE}$ than those with weakened precipitation anomalies (figure 3(b)). In humid regions, although the mean $\Delta\alpha^{PRE}$ is smaller, the mean $\Delta N_2OEA_PRE^{STD}$ is nine times greater in grid cells with $\Delta PRE^{STD} > 0$ than those with $\Delta PRE^{STD} < 0$ (figure 3(e)). We also found that the standard deviation of the anomalies of the globally integrated precipitation over land increased over time during our study period (supplementary figures 6 (d–f)). This increased precipitation variability, driven largely by global warming [10], is one of the drivers enhancing the response of land N₂O emission to precipitation.

In addition, we found that the mean $\Delta N_2OEA_PRE^{STD}$ is 2 (arid), 6 (semi arid), 4 (dry subhumid) and 3 (humid) times higher in grid cells with croplands (see Methods) compared to those without within each aridity class (figure 3(f): supplementary figure 5). With intensive nitrogen fertilizer additions, croplands generally have higher nitrogen substrate that is susceptible to both gaseous and leaching losses. Regions with high emission rates are thus also likely to have high emission anomalies. We then estimated $\Delta N_2OEA_PRE^{STD}$ as a percentage change relative to $N_2OEA_PRE^{STD}$ from the earliest time window. We still found a higher mean $\Delta N_2OEA_PRE^{STD}$ from croplands than non-croplands in arid, semi-arid, dry subhumid and humid regions (supplementary figure 8). This disproportionately higher $\Delta N_2OEA_PRE^{STD}$ from croplands (supplementary figure 5) is most likely linked with more nitrogen surplus from croplands than natural lands. Furthermore, broadly speaking, places with higher cropland fractions or higher



$\alpha^{\text{PRE}} \times \text{Nfert}$ (precipitation anomaly multiplying total mineral nitrogen fertilizer per grid cell) on average have higher α^{PRE} and especially $\text{N}_2\text{OEA_PRE}^{\text{STD}}$ (supplementary table 2), which indicates that nitrogen fertilizer additions interact with precipitation in shaping the pattern of N_2OEA .

Next we investigated whether process-based land N_2O models capture the top-down N_2O -precipitation relationship. To tackle this issue, we calculated α^{PRE} from three global land N_2O models (ORCHIDEE-CNP, ORCHIDEE and OCN) that participated in NMIP and quantified land N_2O emissions with the same temporal resolution as the inversion estimates (Methods). These models however, are bottom-up calculations on land fluxes that are different from observed atmospheric growth rate anomalies. The correlations between globally integrated land N_2OEA and PRE are weaker from land models ($r = 0.32\text{--}0.38$, $P < 0.05$) than from top-down inversions (supplementary figure 9). α^{PRE} increase with time in 2 out of 3 models, but the magnitude of α^{PRE} and its changes are more than three times smaller than from top-down inversions (figure 1 vs. supplementary figure 9). Compared to the globally integrated N_2OEA , agricultural N_2OEA shows a stronger correlation with PRE ($r = 0.42\text{--}0.56$, $P < 0.05$) and higher α^{PRE} (in unit of per area) with the overall increasing trend despite large differences among the three models (supplementary figure 10). The factorial model simulations from NMIP enable us to separate the effect of nitrogen additions by comparing simulations with vs. without external nitrogen inputs (e.g. nitrogen fertilizer, manure and atmospheric nitrogen deposition). Enhanced N_2O emissions from agricultural land are driven largely by external nitrogen inputs, especially nitrogen fertilizer additions [13, 29]. This is supported by process-based model simulations that show the important contribution of agricultural land and therefore anthropogenic nitrogen additions to the intensified N_2O -precipitation relationship. Both process-based models and inverse-estimations show the same tendency for N_2O -precipitation relationship.

The lower sensitivity of N_2OEA to PRE from NMIP models indicates uncertainties in modelling the impacts of precipitation on N_2O emissions, which may stem from difficulties in accurately representing the hydrological processes (from precipitation to soil moisture and water filled pore space) [30], or the soil moisture responses of N_2O emissions. Process-based models generally represent soil moisture effects on N_2O emissions through empirical soil moisture (or water filled pore space) response functions [3, 5, 13, 31]. These functions are typically derived from limited site-level studies, and may not be universal or adequate in capturing the multifaceted soil moisture triggered changes, for example, the rapid microbial responses following rewetting of dry soils [32]. Due to the complexity and relatively high computation requirements, these global N_2O models typically do not simulate nitrifying and denitrifying microbial communities explicitly. Whether the lack of microbial physiology leads to biased simulation of moisture responses remains

to be explored. Note there are limited numbers of process-based global N₂O models [29], and a comprehensive assessment on the capacity to model soil moisture responses requires more effort from both modelers and data collectors. The average correlation between satellite derived soil moisture anomalies (ESACCI v05.2, the combined product) and N₂OEA from atmospheric inversions is 0.27. Satellite derived soil moisture datasets normally only capture first top centimetres of soil, which is not adequate in representing biogeochemical active soil zones. This correlation value reached 0.42 from model estimated soil moisture (CPC soil moisture, one-layer hydrological model) or 0.40 from a reanalysis dataset (ERA5, 0–28 cm). The global scale soil moisture datasets are likely to be associated with higher uncertainties than observation-derived precipitation datasets. While water filled pore space (approximated by soil moisture in models) [5, 13] is a more direct regulator of soil N₂O emissions than precipitation, how to realistically capture its dynamics and impacts on large-scale soil N₂O emissions requires more efforts in the future.

The top-down (atmospheric inversion) and process-based modelling estimates are consistent in terms of the decadal global N₂O budget [14], while the climate sensitivities of land N₂O emissions may need more studies considering the uncertainties in both atmospheric inversions and process-based modelling, and regional scale observations related to this topic are especially in need. N₂O emissions from inland water bodies are not included in NMIP models, but are incorporated in the top-down inversion estimates. We did not remove N₂O emissions from inland water bodies in the top-down estimates due to lack of reliable observations. Estimations of N₂O emissions from inland waters and estuaries remain largely uncertain (Rivers: 0.03–2; Estuaries: 0.06–5.7 Tg N₂O–N yr⁻¹) [33, 34], with one recent modelling study arguing for an overestimation of previous values (Rivers: 0.05; Estuaries: 0.06–0.15 Tg N₂O–N yr⁻¹) [34]. Nitrogen lost through leaching is one of the major sources that contribute to aquatic N₂O emissions [33]. Leaching losses of agricultural nitrogen inputs are closely linked with precipitation. ORCHIDEE-CNP and ORCHIDEE show increased sensitivity of anomalies of nitrogen leaching from agricultural nitrogen additions to PRE (supplementary figure 11), while simulations without agricultural nitrogen additions do not show increasing trends despite the strong correlation between anomalies in nitrogen leaching and PRE (supplementary figure 12, $r = 0.84$, ORCHIDEE-CNP; $r = 0.58$, ORCHIDEE). Agricultural N₂O additions that end up in inland water systems may also play a role in the increasing trend of α^{PRE} and N₂O^{PRE} from atmospheric inversions, although the magnitude is likely to be small considering the relatively small N₂O fluxes from inland waters.

The lack of temperature signal on the global scale N₂O emission anomalies is partly due to spatial aggregation (supplementary figure 13). At the local scale, from gridded inversions fluxes of N₂O, anomalies in temperature and precipitation play approximately equal roles in N₂OEA. The relative importances of temperature and radiation decrease at large spatial scales, while the importance of precipitation remains high. Locally, temperature (or radiation) could have both positive and negative impacts on N₂O emissions (supplementary figure 14). For example, high temperature stimulates nitrifiers and denitrifiers that produce N₂O, while exacerbated soil drying under warming decreases N₂O emissions [35] despite the effect also depends on the interaction with precipitation. Warming reduces substrate availability for nitrification and denitrification through enhancing plant growth and nitrogen uptake, but also boosts nitrogen supply through increased nitrogen mineralization [35]. These positive and negative effects, typically involving complex interactions among spatially diverse climatic, biological, edaphic and anthropogenic factors, compensate in space and result in a small temperature (or radiation) signal at the global scale. In addition, locations with high temperature anomalies are from the northern high latitudes (especially Siberia). In Siberia, the N₂O emission rate is relatively low and inverse estimations are largely uncertain due to very sparse observations. Note here we did not quantify precipitation-temperature interactions, which might be important locally.

Global N₂O emissions have been accelerated over the last two decades, largely driven by anthropogenic activities that intensify the global nitrogen cycle [14, 19]. Interactions between the expedited nitrogen fertilization and intensified precipitation anomalies (associated with global warming) shift land N₂O emissions. We predict land N₂O emissions to be more sensitive to precipitation anomalies in the future under the business-as-usual fertilization practice and high emission climate scenarios. To support 10 billion people in 2050, projected nitrogen fertilizer use will have to increase to 141 Tg N yr⁻¹ (from 107 TgN yr⁻¹ in 2015) under the business-as-usual practice [1]. The standard deviation of PRE is 42%, 36% and 26% higher by the end of 21st century under the SSP5-85 (Shared Socioeconomic Pathways with a radiative forcing of 8.5 Wm⁻² in 2100), SSP3-70 (radiative forcing: 7.0 Wm⁻²) and SSP2-45 (radiative forcing: 4.5 Wm⁻²), respectively, from an ensemble of Earth system simulations (supplementary figure 15). Only under the sustainable pathway, SSP1-26 (radiative forcing: 2.6 Wm⁻²), the standard deviation of PRE is not increased by the end of this century. The tendency of global aridification and the expansion of the world's dryland under future warming climate [36, 37] also indicate a higher sensitivity of future land N₂O emissions to precipitation. We call for special attention on N₂O emissions in farming of the semi-arid land, which

could contribute to disproportionately high N₂O emissions (per unit area) under its precipitation variabilities.

Despite the robustness of the overall global trends, our understanding of the mechanism(s) driving enhancements of α^{PRE} and N₂OEA_PRE is still limited. We demonstrated the intensifying agricultural nitrogen inputs as an important mechanism, but precise data on large-scale mineral fertilizer and manure addition (especially the timing of applications) are lacking. Coordinated efforts on monitoring agricultural nitrogen inputs are in great need. Many factors and types of disturbance, such as crop harvesting, soil tillage and earthworm activity, could trigger local or temporal nitrogen surplus and N₂O emission anomalies. Whether these factors are regionally or globally important remain to be studied. Here as a first step, we revealed the general relationship between land N₂O emissions and precipitation anomalies, and focused on the most critical factors at the global scale, while acknowledging many questions (e.g. differences among countries/biomes/land uses) in this subject remain to be answered. We need more attention and community efforts dedicated to monitor land N₂O emission (with its covariates) and to improve process-based understanding of N₂O dynamics.

4. Conclusions

Through the top-down estimates of land N₂O emissions from three independent atmospheric inversion systems, we found a significant correlation ($P < 0.001$) between the interannual anomalies in the annual growth rate of the global land N₂O emissions and precipitation anomalies. The average sensitivity (α^{PRE}) was 2.50 ± 0.98 Tg N₂O–N per 100 mm of precipitation across the global land between 1998 and 2016. α^{PRE} increased with time during 1998–2016, likely due to enhanced precipitation anomalies interacting with increased nitrogen inputs to agricultural lands. α^{PRE} generally increases with aridity and under future climate conditions (with radiative forcing levels of 4.5, 7.0 and 8.5 Wm⁻² by the year 2100).

Data availability statement

The data that support the findings of this study are openly available at the following URL/DOI [38]: <https://figshare.com/s/2deaae350b24a7c1bcd8>.

Code availability

Calculations were conducted through Python 3.7.3, R 3.6.2 and ferret 6.72. Data processing code and code used to generate figures are provided at <https://figshare.com/s/2deaae350b24a7c1bcd8>.

Acknowledgments

We acknowledge research groups and institutes provide atmospheric N₂O inversions, process-based N₂O modelings, atmospheric N₂O measurements and climate datasets. We especially thank Rona L Thompson for providing publicly available atmospheric inversion datasets for N₂O. P C, O B and Y H. This work benefited from the French state aid managed by the ANR under the ‘Investissements d’avenir’ programme with the reference ANR-16-CONV-0003. The LMDz modelling results were funded through the Copernicus Atmosphere Monitoring Service (<https://atmosphere.copernicus.eu/>), implemented by ECMWF on behalf of the European Commission, and were generated using computing resources from LSCE.

Conflict of interest

The authors declare no competing interests.

Author contributions

P C, O B and Y H designed this study. R L T, H T, F Z, J C, S H and N P contributed the data. P C, O B, Y W and Y H discussed analyzing methods. Y H conducted the analysis. Y H, P C and O B drafted the manuscript. All authors discussed the results and contributed to writing the manuscript.

ORCID iDs

Yuanyuan Huang  <https://orcid.org/0000-0003-4202-8071>
Philippe Ciais  <https://orcid.org/0000-0001-8560-4943>

Ying-Ping Wang  <https://orcid.org/0000-0002-4614-6203>
Hanqin Tian  <https://orcid.org/0000-0002-1806-4091>
Feng Zhou  <https://orcid.org/0000-0001-6122-0611>
Jinfeng Chang  <https://orcid.org/0000-0003-4463-7778>
Hao Shi  <https://orcid.org/0000-0001-8250-0567>
Shu Kee Lam  <https://orcid.org/0000-0001-7943-5004>

References

- [1] Davidson E A 2012 Representative concentration pathways and mitigation scenarios for nitrous oxide *Environ. Res. Lett.* **7** 024005
- [2] Hu H W, Chen D and He J Z 2015 Microbial regulation of terrestrial nitrous oxide formation: understanding the biological pathways for prediction of emission rates *FEMS Microbiol. Rev.* **39** 729–49
- [3] Li C S, Frolking S and Frolking T A 1992 A model of nitrous-oxide evolution from soil driven by rainfall events.1. Model structure and sensitivity *J. Geophys. Res.* **97** 9759–76
- [4] Griffis T J, Chen Z, Baker J M, Wood J D, Millet D B, Lee X, Venterea R T and Turner P A 2017 Nitrous oxide emissions are enhanced in a warmer and wetter world *Proc. Natl Acad. Sci. USA* **114** 12081–5
- [5] Huang Y and Gerber S 2015 Global soil nitrous oxide emissions in a dynamic carbon-nitrogen model *Biogeosciences* **12** 6405–27
- [6] Wang Q H et al 2020 Data-driven estimates of global nitrous oxide emissions from croplands *Natl Sci. Rev.* **7** 441–52
- [7] Dobbie K E and Smith K A 2003 Nitrous oxide emission factors for agricultural soils in Great Britain: the impact of soil water-filled pore space and other controlling variables *Glob. Change Biol.* **9** 204–18
- [8] Wagner-Riddle C, Baggs E M, Clough T J, Fuchs K and Petersen S O 2020 Mitigation of nitrous oxide emissions in the context of nitrogen loss reduction from agroecosystems: managing hot spots and hot moments *Curr. Opin. Environ. Sustain.* **47** 46–53
- [9] He X G and Sheffield J 2020 lagged compound occurrence of droughts and pluvials globally over the past seven decades *Geophys. Res. Lett.* **47** e2020GL087924
- [10] Dai A G 2013 Increasing drought under global warming in observations and models *Nat. Clim. Change* **3** 52–58
- [11] Harris E et al 2021 Denitrifying pathways dominate nitrous oxide emissions from managed grassland during drought and rewetting *Sci. Adv.* **7** eabb7118
- [12] Congreves K A, Wagner-Riddle C, Si B C and Clough T J 2018 Nitrous oxide emissions and biogeochemical responses to soil freezing-thawing and drying-wetting *Soil Biol. Biochem.* **117** 5–15
- [13] Tian H Q et al 2018 The global N₂O model intercomparison project *Bull. Am. Meteorol. Soc.* **99** 1231–52
- [14] Tian H Q et al 2020 A comprehensive quantification of global nitrous oxide sources and sinks *Nature* **586** 248–56
- [15] Firestone M K and Davidson E A 1989 Microbiological basis of NO and N₂O production and consumption in soil *Exchange of Trace Gases between Terrestrial Ecosystems and the Atmosphere* ed M O Andreae and D S Schimel (New York: Wiley) pp 7–21
- [16] Linn D M and Doran J W 1984 Effect of water-filled pore space on carbon dioxide and nitrous oxide production in tilled and nontilled soils *Soil Sci. Soc. Am. J.* **48** 1267–72
- [17] Davidson E A, Keller M, Erickson H E, Verchot L V and Veldkamp E 2000 Testing a conceptual model of soil emissions of nitrous and nitric oxides *Bioscience* **50** 667–80
- [18] Parn J et al 2018 Nitrogen-rich organic soils under warm well-drained conditions are global nitrous oxide emission hotspots *Nat. Commun.* **9** 1–8
- [19] Thompson R L et al 2019 Acceleration of global N₂O emissions seen from two decades of atmospheric inversion *Nat. Clim. Change* **9** 993–8
- [20] Wang X H et al 2014 A two-fold increase of carbon cycle sensitivity to tropical temperature variations *Nature* **506** 212–5
- [21] Gutschow J, Jeffery M L, Gieseke R, Gebel R, Stevens D, Krapp M and Rocha M 2016 The PRIMAP-hist national historical emissions time series *Earth Syst. Sci. Data* **8** 571–603
- [22] Lu C Q and Tian H Q 2017 Global nitrogen and phosphorus fertilizer use for agriculture production in the past half century: shifted hot spots and nutrient imbalance *Earth Syst. Sci. Data* **9** 181–92
- [23] Harris I C, Jones P D and Osborn T (University of East Anglia Climatic Research Unit) 2020 CRU TS4.04: Climatic Research Unit (CRU) Time-Series (TS) version 4.04 of high-resolution gridded data of month-by-month variation in climate (Jan. 1901–Dec. 2019) (Centre for Environmental Data Analysis) (available at: <https://catalogue.ceda.ac.uk/uuid/89e1e34ec3554dc98594a5732622bce9>)
- [24] Trabucco A and Zomer R J 2019 Global aridity index and potential evapotranspiration (ET0) climate database v2 (Dataset) (available at: <https://cgiiarcsi.community/2019/01/24/global-aridity-index-and-potential-evapotranspiration-climate-database-v2/>)
- [25] United Nations Environment Programme 1992 World Atlas of Desertification (London: UNEP)
- [26] O'Neill B C et al 2016 The scenario model intercomparison project (ScenarioMIP) for CMIP6 *Geosci. Model. Dev.* **9** 3461–82
- [27] Jung M et al 2017 Compensatory water effects link yearly global land CO₂ sink changes to temperature *Nature* **541** 516–20
- [28] Goldewijk K K, Beusen A, Doelman J and Stehfest E 2017 Anthropogenic land use estimates for the Holocene - HYDE 3.2 *Earth Syst. Sci. Data* **9** 927–53
- [29] Tian H Q et al 2019 Global soil nitrous oxide emissions since the preindustrial era estimated by an ensemble of terrestrial biosphere models: magnitude, attribution, and uncertainty *Glob. Change Biol.* **25** 640–59
- [30] Huang Y Y, Gerber S, Huang T Y and Lichstein J W 2016 Evaluating the drought response of CMIP5 models using global gross primary productivity, leaf area, precipitation, and soil moisture data *Glob. Biogeochem. Cycles* **30** 1827–46
- [31] Zaehle S, Ciais P, Friend A D and Prieur V 2011 Carbon benefits of anthropogenic reactive nitrogen offset by nitrous oxide emissions *Nat. Geosci.* **4** 601–5
- [32] Rudaz A O, Davidson E A and Firestone M K 1991 Sources of nitrous-oxide production following wetting of dry soil *FEMS Microbiol. Ecol.* **85** 117–24
- [33] Yao Y Z, Tian H, Shi H, Pan S, Xu R, Pan N and Canadell J G 2020 Increased global nitrous oxide emissions from streams and rivers in the anthropocene *Nat. Clim. Change* **10** 138–42
- [34] Maavara T, Lauerwald R, Laruelle G G, Akbarzadeh Z, Bouskill N J, Van Cappellen P and Regnier P 2019 Nitrous oxide emissions from inland waters: are IPCC estimates too high? *Glob. Change Biol.* **25** 473–88
- [35] Dijkstra F A, Prior S A, Runion G B, Torbert H A, Tian H, Lu C and Venterea R T 2012 Effects of elevated carbon dioxide and increased temperature on methane and nitrous oxide fluxes: evidence from field experiments *Front. Ecol. Environ.* **10** 520–7

- [36] Berg A *et al* 2016 Land-atmosphere feedbacks amplify aridity increase over land under global warming *Nat. Clim. Change* **6** 869–74
- [37] Chai R, Mao J, Chen H, Wang Y, Shi X, Jin M, Zhao T, Hoffman F M, Ricciuto D M and Wullschleger S D 2021 Human-caused long-term changes in global aridity *npj Clim. Atmos. Sci.* **4** 65
- [38] Huang Y, Ciais P, Boucher O, Boucher Y, Tian H and Zhou F 2022 Code and data for: increasing sensitivity of terrestrial nitrous oxide emissions to precipitation variations *figshare* (Dataset) (<https://doi.org/10.6084/m9.figshare.16344837.v1>)